Synoptic forcing of the Korea Strait transport

G.A. Jacobs[a,*], D.S. Ko[a], H. Ngodock[b], R.H. Preller[a], S.K. Riedlinger[a]

[a]*Naval Research Laboratory, Stennis Space Center, MS, USA*
[b]*University of Southern Mississippi, Stennis Space Center, MS, USA*

Abstract

Korea Strait transport variations in the synoptic frequency band (2–20 days) are examined using results of a numerical 3-D primitive equation model, satellite observed sea-level variations, a linear barotropic adjoint dynamic model, and observed transports. The 3-D numerical model does not assimilate observations, and the agreement with the observed transport implies that wind forcing is one of the main contributors to variations in the synoptic band. The satellite-observed and 3-D model sea-level indicate a sea-level response to wind stress along the east Korean coast that propagates toward the Korea Strait and changes the sea-level slope across the strait. The adjoint results indicate that wind stress is most influential in the area east of Korea along with secondarily important area along the East China Sea shelf break south of Japan. The mechanism connecting wind stress to transport variations is a Kelvin wave propagation that changes sea-level slope across the strait, leading to the altered geostrophic transport through the strait. A strong southerly wind initially produces a sea-level set down along the east Korea coast and a sea-level increase along the shelf break. The set down propagates to the Korea Strait as a Kelvin wave, sea level across the strait changes, and the transport through the strait increases. Similarly, northerly wind stress produces a set up along the Korea coast and subsequent decreased transport. Wind stresses across the Yellow and East China Seas are not a significant forcing mechanism since Kelvin waves would propagate away from the strait. Barotropic transport response to wind stress is rapid (on the order of 3 h), but the relatively slow development of the atmospheric forcing (on the order of 1–2 days) modulates the response.
Published by Elsevier Ltd.

1. Introduction

The Korea Strait transport provides the largest portion of horizontal heat and salt flux to the environment in the Japan/East Sea (JES). The relatively warm fresh inflow to the JES forms a surface layer in the summer and strengthens the anticyclonic circulation south of the subpolar front. Because the strait is shallow (depths less than 150 m), it would be expected that local wind stress could have a large impact on transport. Mizuno et al. (1986) examine the correlation between one current-meter mooring along the Japan coast in the strait to the wind stress at the same point. A correlation between currents and

*Corresponding author.

E-mail address: jacobs@nrlssc.navy.mil (G.A. Jacobs).

wind stress exists, though statistical significance is minor. The shallow adjoining Yellow and East China Seas continental shelf has been observed to respond to wind stress with sea level changes on the order of 1 m (Hsueh, 1988; Jacobs et al., 1998). Sea-level differences between the upstream and downstream sides of the strait would produce pressure gradients across the strait that could change transport (Ohshima, 1994). Thus, there are a number of physical mechanisms through which wind stress may influence the strait transport. The analysis here provides support to determine the dominant mechanism connecting wind stress to the strait transport variations.

The transport variation time scales greatly impact the primary mechanism connecting the forcing to the transport variation. Different dynamics dominate at different time scales. At seasonal to interannual scales, it is expected that the sea-level drop across the strait determines the transport, and the Pacific Ocean circulation controls the sea-level difference between the inflow and outflow of the JES. This study is concerned with the short time scales at which it is expected that synoptic wind events influence the transport fluctuations. For purposes here, we define the synoptic time scale to include variations on periods from 2 to 20 days. On longer time scales (seasonal to annual), wind stress changes the North Pacific subtropical gyre circulation as well as the subpolar gyre circulation. These in turn impact the sea level south of Japan at the inflow to the JES and at the Tsugaru Strait at the JES outflow.

The design of different analyses must differentiate between the many possible mechanisms through which the wind stress may influence the strait transport. Because of the difficulty in using analytic tools with the realistic regional topography and geometry, the principal tools at our disposal are observations and numerical models. To provide some insight to the problem at hand, observed strait transport is correlated to the wind stress and sea level throughout the area. One problem that becomes clear is that the coupling between simple analyses such as correlation analysis and the large-scale nature of the wind stress confounds our ability to clearly differentiate forcing mechanisms and reach definitive conclu-

sions. Wind stress at one point may be very influential to the strait transport, and the wind stress at a second point may be dynamically irrelevant. However, the wind stress at the two points may be strongly correlated due to the large-scale nature of the atmosphere. Thus, the dynamically irrelevant point may appear to be strongly correlated to transport variations in the strait. Similarly, because the atmospheric pressure and winds stress are closely related through geostrophy, correlation analysis is not able to demonstrate the more important of these two driving forces. To clearly divide the influential wind stress areas from the irrelevant, it is necessary to compute the sensitivity of transport to the wind stress throughout the area. The sensitivity may be constructed by computing the derivative of transport with respect to the wind stress throughout the area, and the correlation analysis provides only an indirect indication of this value. An adjoint model is capable of computing this sensitivity directly and provides a demonstration of the strait transport sensitivity to the wind stress as determined by the prescribed dynamics of the adjoint model. This study employs a barotropic adjoint model. The large-scale nature of the wind stress no longer impedes progress. Of course, it must be kept in mind that the sensitivity elucidated by the adjoint model is entirely dependent upon the dynamics prescribed within the model, and the adjoint model employed here is relatively simple.

2. Data sources

The Navy Coastal Ocean Model (NCOM) can be set up as a hybrid sigma (terrain-following) and Z (fixed depth) level coordinate system. In the study here, NCOM is implemented in purely sigma mode and is thus similar to the Princeton Ocean Model (POM) (Blumberg and Mellor, 1987). This NCOM provides the numerical model transports for this study. The main difference between the present model and POM is that the forward time stepping is an implicit scheme. The implicit numerical scheme maintains stability even with much larger time steps (Martin, 2000). This allows computation of the internal and external modes at

the same time steps rather than implementing the mode splitting scheme used in POM. The model results presented here use the Mellor–Yamada level 2.0 turbulence closure scheme (Mellor and Yamada, 1974). The East Asian Seas (EAS) model covers the South China Sea through the JES at 1/8° horizontal resolution (Fig. 1) so that boundary conditions do not exist at straits connecting the marginal seas. However, the EAS model east boundary is open, and the model requires realistic conditions at these boundaries.

To provide the open-boundary conditions, a courser-resolution model is constructed covering the north Pacific north of 20°S at 1/4° horizontal resolution and 26 sigma levels. The southern boundary is closed. Subsurface temperature and salinity are initialized from the Modular Ocean Data Assimilation System (MODAS) climatology (Fox et al., 2002). The large North Pacific domain model is spun up from 1992 and run to 2001 forced by wind stress and heat flux from the Navy

Operational Global Atmospheric Prediction System (NOGAPS) (Hogan and Rosmond, 1991; Rosmond, 1992; Hogan, 1993). Subsurface temperature and salinity are relaxed to the MODAS climatology on a 250-day e-folding time scale, which should not affect the synoptic frequencies examined here. Boundary conditions from the large domain model are then provided to the EAS model, and the EAS model is run from 1994 through 2001 forced by the same wind stress, heat flux, and relaxation to climatological subsurface temperature and salinity as is used in the larger domain coarse-resolution model.

The transport through the Korea Strait is computed from the model velocity and band-pass filtered using two Bartlett filters with first 0 power points at 2 days and then at 20 days (Fig. 2). A time series of observed transport is provided from acoustic Doppler current profilers (ADCPs) moored along a line spanning the strait southwest of Tsushima Island (Perkins et al., 2000). The deployment time period covers May 1999 through February 2000. The numerical model experiment results cover the observation period. Jacobs et al. (2001) discuss the transport estimation from these instruments. The observed transport time series is filtered by the same method as the model transport. The model contains many of the short period transport variations observed in the strait.

The TOPEX/POSEIDON (T/P) satellite (Fu et al., 1994) provides the altimeter data used here. The data are processed as described in Jacobs et al. (1998). Tides are the largest contributor to sea-level variations in this region, and careful attention is given to the tide estimation and removal. After a harmonic analysis of the principal eight tide constituents directly from the data, Jacobs et al. (1998) examine the residual variability, which is dominated by wind-driven sea-level change. Even though other altimeter data sets such as those obtained by the ERS-2 satellite are much more spatially dense, the T/P ground tracks are sampled every 9.95 days as opposed to 35 days by ERS-2. With a short time series of observed transport (only 10 months), as many sea-level observations as possible are needed to improve statistical significance. Thus, this analysis uses only the T/P data.
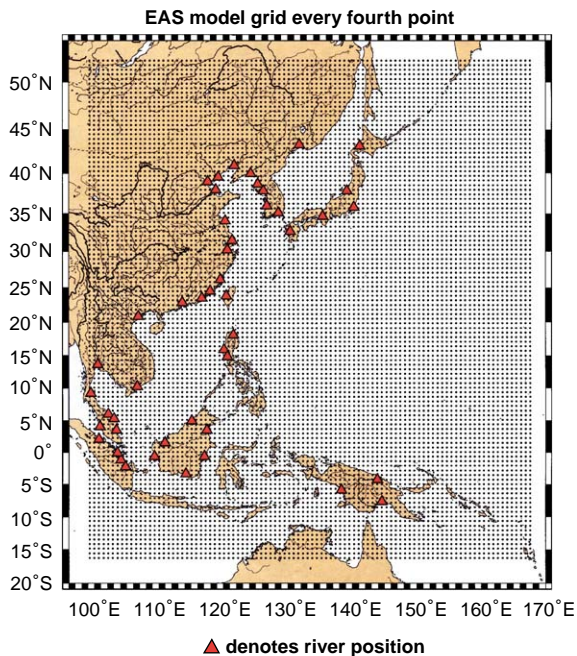
Fig. 1. The East Asian Seas NCOM model that provides the transport variations for this study is embedded within a large-domain model that provides boundary condition transport, temperature, and salinity.
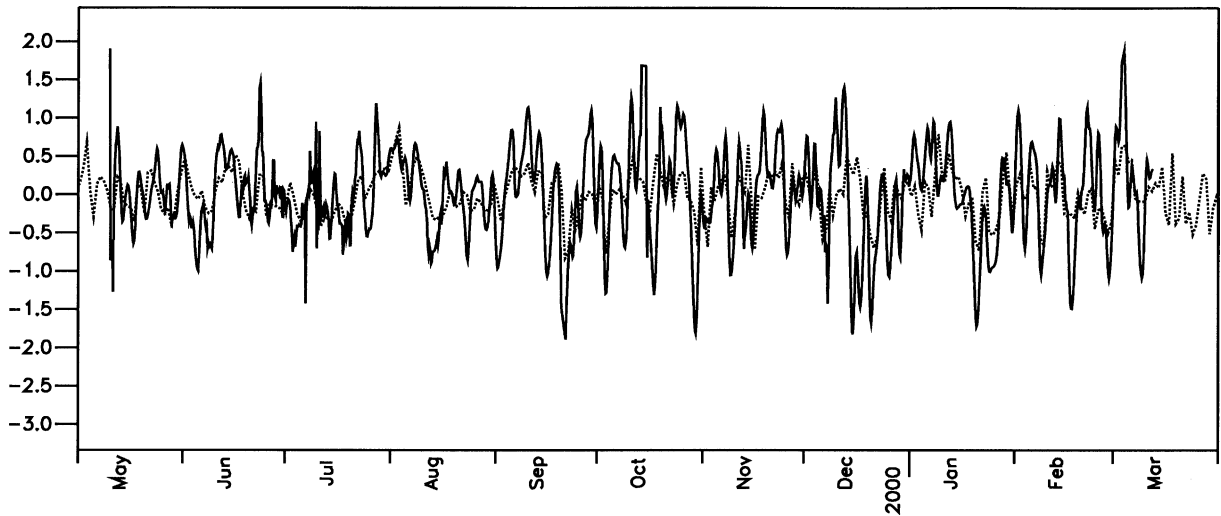
Fig. 2. The EAS numerical model (dashed) and observed transport (solid) through the Korea Strait are filtered to the synoptic band (2–20) days for direct comparison. Most of the transport events observed in the strait are reproduced in the model. These would be expected to be deterministically wind forced processes, and this indicates skill in the wind-forcing as well as the model dynamics.

3. Cross-covariance analyses

The NCOM and observed transports are filtered to the synoptic periods (Fig. 2). Most of the short time period features observed by the mooring array are reproduced by the numerical model. This implies accuracy of both the wind-stress field and the NCOM dynamics linking the wind stress to the transport. Some features are not reproduced well in the numerical model. These may be due to inaccuracies in the wind stress, inaccuracies in the model dynamics or nondeterministic features. The ocean mesoscale in particular is nondeterministic, and the numerical model used here does not assimilate any observations that would provide the synoptic mesoscale. The agreement between the observed and NCOM transports immediately implies that deterministic surface fluxes are the main source leading to transport variations through the strait.

In this analysis the time-lagged covariance is computed between the transport and the wind-stress components at each point in space. The covariance of observed transport to the NOGAPS x wind stress and the covariance to the y wind stress may be plotted as a vector at each point

(Fig. 3). Similarly, the lagged covariance of NCOM transport to the time series of x and y wind-stress time series is computed (Fig. 4). A statistical significance test must be conducted to determine a confidence level in the results. The significance test is applied independently to each wind-stress component at each point in space. The variance of the distribution of the cross-covariance is computed by

$$\operatorname{var}(R_{fg}) = \int\limits_0^T \int\limits_0^T \big[R_{ff}(v-u) R_{gg}(v-u) \\ + R_{fg}(v-u) R_{fg}(v-u) \big]\, du\, dv, \qquad (1)$$

where R_{fg} is the cross covariance between the time series f and g and T is the total time period covered by the lagged time series (Bendat and Piersol, 1986). The lagged autocovariances R_{ff} and R_{gg} are represented by Gaussian functions. The e-folding length scales are estimated from the actual lagged autocovariances.

The square root of the variance (the square root of Eq. (1)) provides the significance limits for a confidence test. That is, the two time series have a non-zero cross-covariance with a confidence
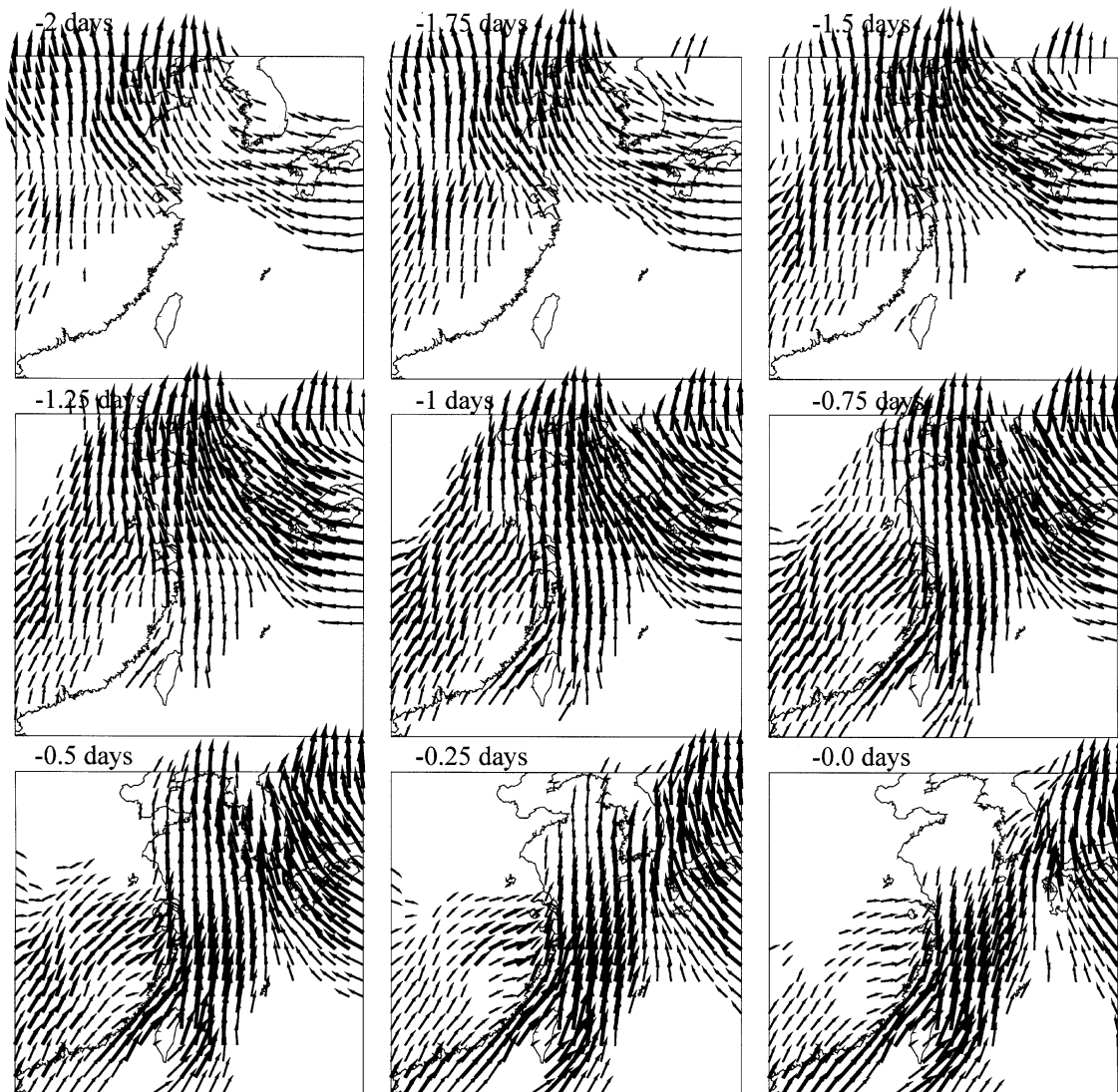
Fig. 3. The covariance of observed transport (Fig. 2) to wind stress is computed at each point in space. The vector components here represent the transport covariance to the zonal and meridional wind stress components at the specified lag. Increasing magnitude lag indicates that the wind variation precedes the transport variation. The line thickness indicates significance level. Covariances under 1 standard deviation of significance are not plotted, covariances up to 2 standard deviations are plotted with thin arrows, covariances from 2 to 3 standard deviations by medium arrows, and covariances above 3 standard deviations are plotted with thick arrows. The transport variations are mostly related to north–south wind stress variations across the Yellow, East China, and Japan/East Seas between −0.5- and −1- day lag (wind stress preceding the transport).

determined by the number of standard deviations given by (1). The cross-covariance plots contain the information on the significance. If the cross-covariance of wind stress and the transport is below 1 standard deviation then a vector is not

plotted in Figs. 3 and 4. Covariances from 1 to 2 standard deviations are plotted by a thin vector, covariances between 2 and 3 standard deviations by a medium thickness vector, and covariances above 3 standard deviations by a thick vector. The
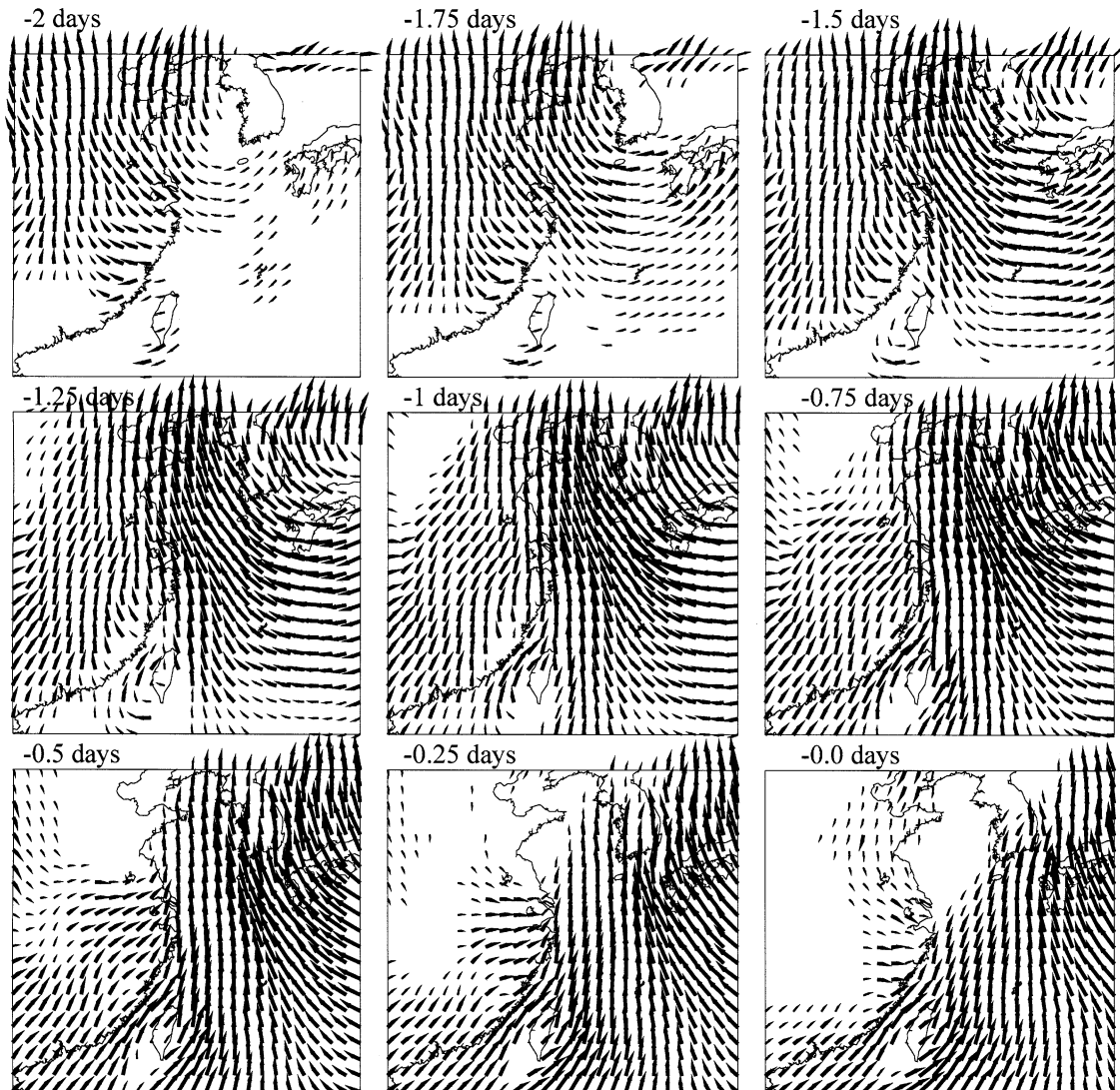
Fig. 4. The same as Fig. 3, but the cross-covariance is between the modeled transport time series and the wind-stress field. The results are similar. Differences are that the significance levels are higher due to the absence of noise in the modeled transport time series. Also, inaccuracies in the wind field would not affect the modeled transport cross-covariance with wind stress as much as the observed transport cross-covariance with wind stress.

significance level computation of the lagged time series follows the same methodology as described above, except that the time series are lagged before computing the e-folding scales and covariance estimates.

Expected variance of the cross-covariance between the transport and the T/P sea level time series may be obtained as described above. However, because the T/P altimeter 10-day time sampling is generally greater than the time scales of variability, the measurements are taken to be statistically independent. Thus, the variance of t he cross-covariance is simply variance divided by the number of samples. The analysis of cross-
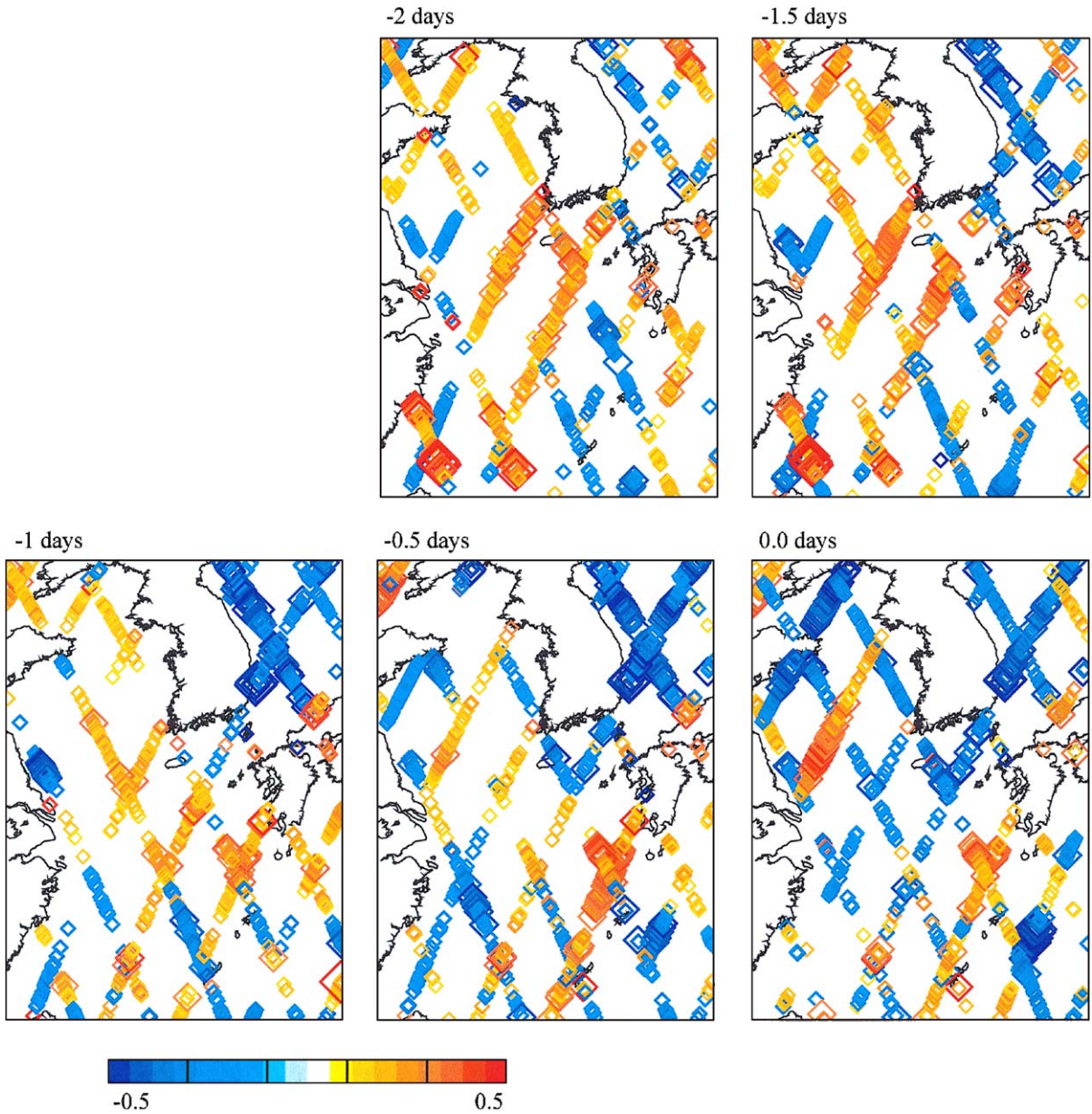
Plate 1. The lagged correlation between the sea level observed by the T/P satellite and the observed transport through the strait is indicated by the color. Correlations less than 1 standard deviation are not plotted. The symbol size indicates the confidence level, with small symbols being 1–2 standard deviations, medium-sized symbols 2–3 standard deviations, and large symbols greater than 3 standard deviations. The most significant correlation occurs at lags of –0.5 to –1.0 days (sea level precedes transport) off the east Korea coast with low sea level preceding transport increases.

covariance and significance is computed separately at each point of the altimeter ground track. Significance is presented by the size of the plotting symbol (Plate 1). Values less than 1 standard deviation are not plotted, values from 1 to 2 standard deviations are plotted by small

diamonds, values from 2 to 3 are plotted by medium diamonds, and values above 3 are plotted by large diamonds.

The correlation of the T/P observed SSH and transport is interpolated spatially by a simple weighted averaging technique. The weighting is a Gaussian function with spatial scales of 75 km. The resulting interpolated correlation (Plate 2) is more easily compared to the numerical model results. The number of observed SSH samples used in the
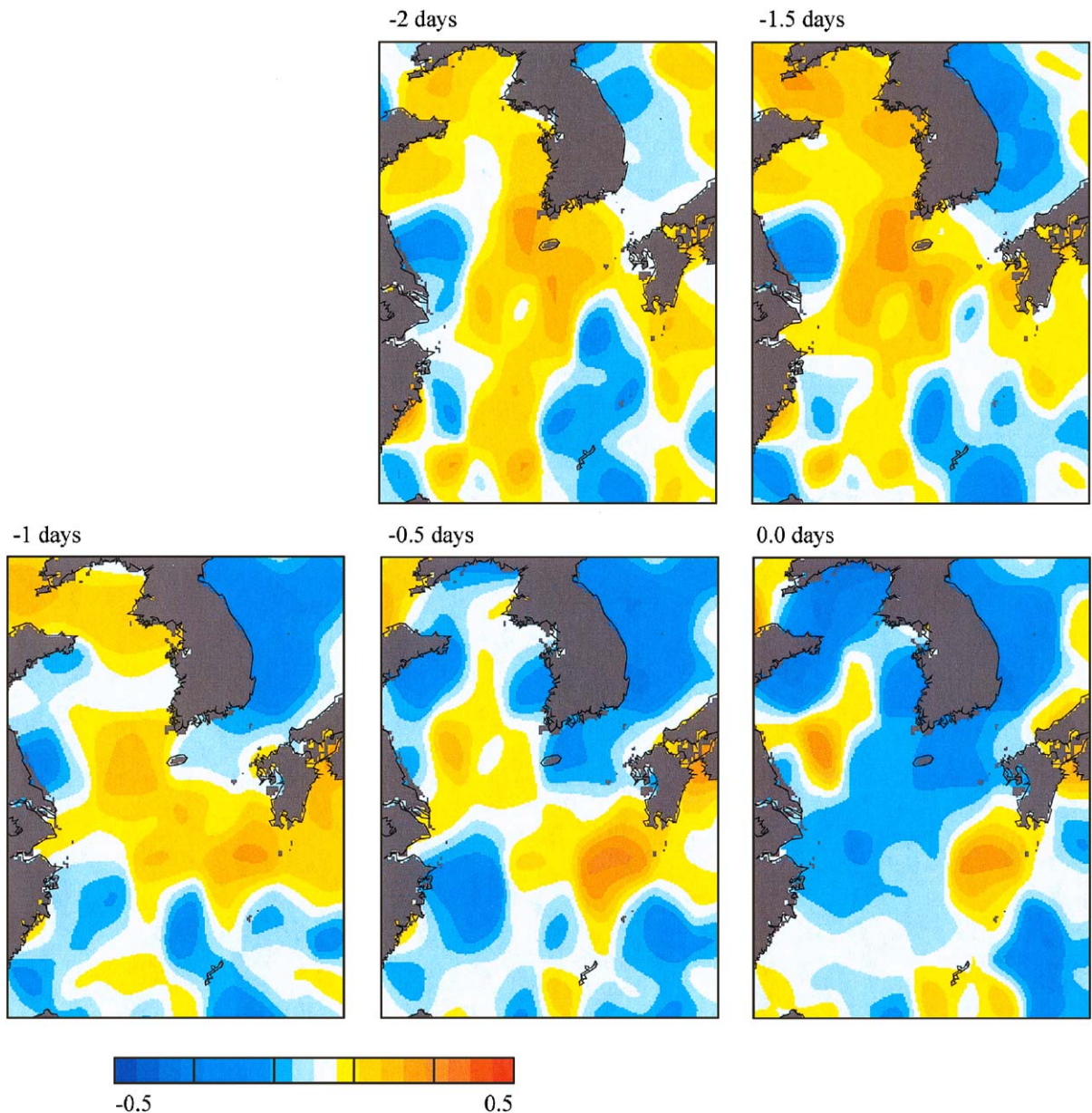
Plate 2. The lagged correlation between the sea level observed by the T/P satellite and the observed transport through the strait after a simple interpolation. The spatial sampling is coarse, but the interpolation aids in comparison with the model results (Plate 3).
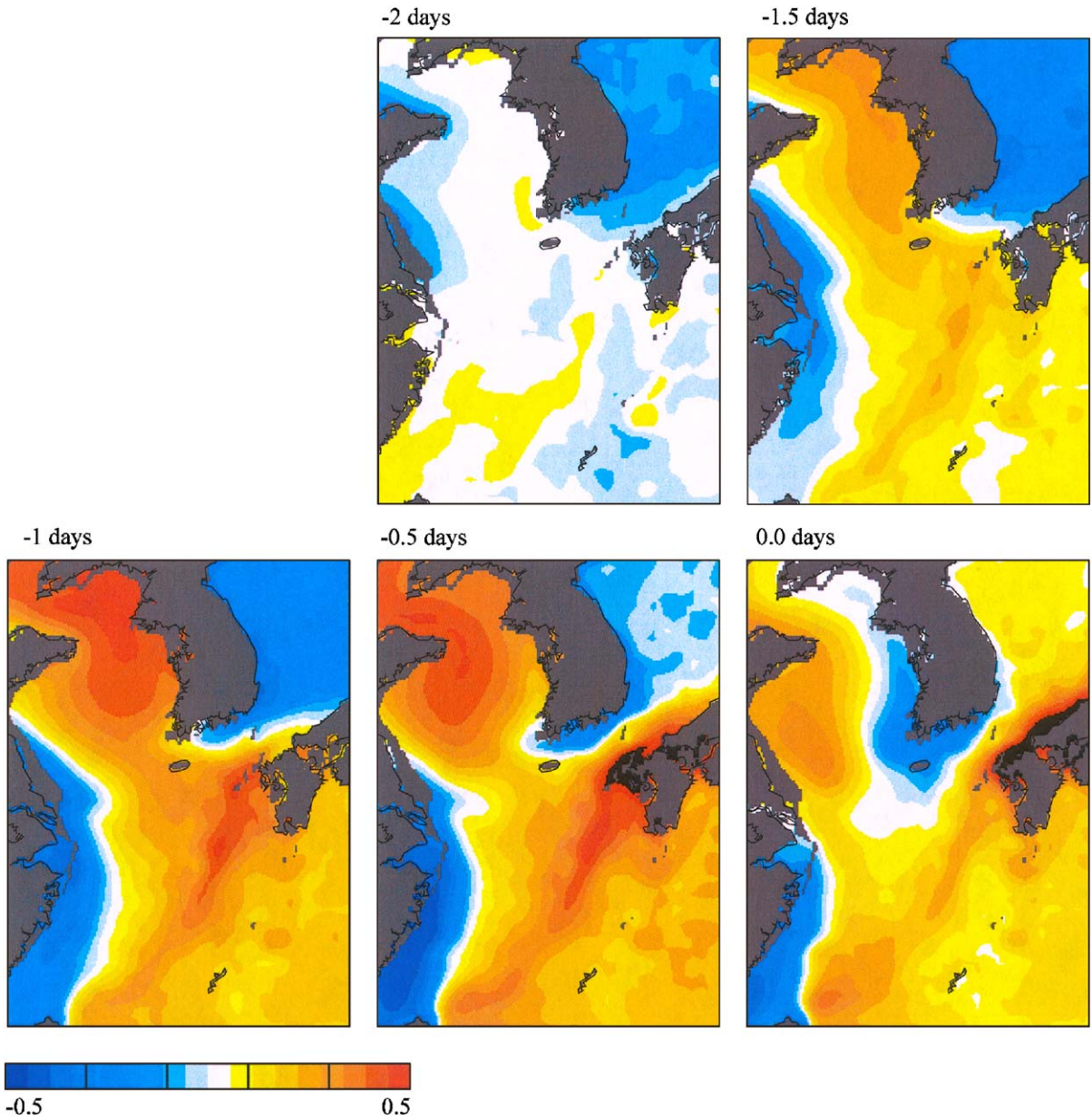
Plate 3. The lagged correlation between the numerical model sea level and the transport through the strait is indicated by the color. The area of greatest correlation propagates from the east Korea coast to the south Korea coast. This propagation is in line with dynamics of Kelvin waves or shelf waves. The sea-level change across the Korea Strait is expected to generate an increased geostrophic transport. A sea-level increase is also present along the shelf break of the East China Sea, which is in the region of wind sensitivity indicated by the adjoint model (Plate 4).

analysis (about 30) is relatively small. Thus, the noise level of the results presented in Plates 1 and 2 is large and significance is generally small.

The model sea level and model transport lagged cross-covariance (Plate 3) provides a good examination of the small spatial scales relating the two

parameters. The correlation between the T/P observed SSH and transport (Plates 1 and 2) must be used with expected error bounds to determine if the model correlations (Plate 3) are in agreement. The largest problem in this comparison is again the small number of SSH samples from the altimeter. In general the negative correlation within the JES along the Korea coast from -1.5 to -0.5 days lag is present in both results. Another feature correlated to a lesser extent is the positive correlation southwest of Kyushu along the shelf break from -0.5 to 0 days lag.

4. The Adjoint

Given a numerical model, let the vector $\mathbf{x}$ contain the model state, which includes all variables (including forcing values such as wind stress) at all points in time and space. Also, let an observation of the state be given by a linear combination of state variables. Thus an observation may be given by $J = \langle \mathbf{H}, \mathbf{x} \rangle$, where the vector $\mathbf{H}$ provides the weights of the state vector elements that contribute to the measurement J, and the brackets indicate an inner product. For example, for an observation of velocity at one point, the measurement function $\mathbf{H}$ would be a vector with all zeroes except for one value of 1. The adjoint provides the derivative of the observation J with respect to the entire model state $\mathbf{x}$ including the input forcing (Marchuk, 1994). If the measurement is of the transport through the Korea Strait then the adjoint can answer the question: what is the derivative of transport with respect to wind stress over all space and time? This provides an understanding of areas in which the wind stress is most influential to controlling the transport through the strait.

For the problem at hand, the parameter of interest is the total transport through the Korea Strait, which is the line integral of transport between two points across the strait. The linear functional $\mathbf{H}$ is defined as the line integral including a certain set of points (i,j) on a numerical C-grid. So then

$$J = \sum_{i,j} \left[u_{i,j}^0 \frac{(H_{i-1,j} + H_{i,j})}{2} \, dx \right.$$
$$\left. + v_{i,j}^0 \frac{(H_{i,j-1} + H_{i,j})}{2} \, dy \right].$$

It is also possible to compute the derivative of J with respect to wind stress at a particular point by using a forward model. To determine the derivative via the forward model, perturb one component of wind stress slightly at one point in space and time, run the model forward, and examine the change in transport. The procedure would be repeated for each component of wind stress at every point and at every time in the model domain. Such a computation would require a number of forward runs equal to the number of model grid points times the number of time lags to be examined, which is prohibitively costly. The adjoint solution requires only one run and thus simplifies the processes of computing the sensitivity.

A demonstration that the adjoint provides the derivative with respect to the model state follows. Let the numerical model state $\mathbf{x}$ be a solution to $\mathbf{A}\mathbf{x} = \tau$ or $\mathbf{A}\mathbf{x} - \tau = 0$, where $\mathbf{A}$ represents the model dynamics and τ the input forcing (which includes input boundary conditions and initial conditions). Suppose there is a dynamical operator $\mathbf{A}^*$ such that $\langle \mathbf{A}\mathbf{x}, \mathbf{H} \rangle = \langle \mathbf{x}, \mathbf{A}^*\mathbf{H} \rangle$. $\mathbf{A}^*$ is then the adjoint operator to $\mathbf{A}$. If the operator $\mathbf{A}$ is a matrix (as in a numerical model) then it may be proven that $\mathbf{A}^* = \mathbf{A}^{\mathbf{T}}$. Let $\mathbf{x}^*$ be a solution to $\mathbf{A}^*\mathbf{x}^* = \mathbf{H}$ or $\mathbf{A}^*\mathbf{x}^* - \mathbf{H} = 0$. Then (after Marchuk, 1994)

$$\langle \mathbf{A}\mathbf{x} - \tau, \mathbf{x}^* \rangle - \langle \mathbf{A}^*\mathbf{x}^* - \mathbf{H}, \mathbf{x} \rangle$$
$$= 0$$
$$= \langle \mathbf{A}\mathbf{x}, \mathbf{x}^* \rangle - \langle \mathbf{A}^*\mathbf{x}^*, \mathbf{x} \rangle + \langle -\tau, \mathbf{x}^* \rangle - \langle -\mathbf{H}, \mathbf{x} \rangle$$
$$= \langle \mathbf{x}, \mathbf{A}^*\mathbf{x}^* \rangle - \langle \mathbf{A}^*\mathbf{x}^*, \mathbf{x} \rangle + \langle -\tau, \mathbf{x}^* \rangle - \langle -\mathbf{H}, \mathbf{x} \rangle$$
$$= \langle -\tau, \mathbf{x}^* \rangle - \langle -\mathbf{H}, \mathbf{x} \rangle$$

and thus $J = \langle \mathbf{H}, \mathbf{x} \rangle = \langle \tau, \mathbf{x}^* \rangle$. The derivative of J with respect to a particular element of τ (wind stress at a particular point in time and space) is simply the value of the adjoint variable at the same point in time and space.

Instead of making many perturbed forward model experiments, one execution of the adjoint model forced by the measurement function $\mathbf{H}$ provides the same information. The ocean dynamics are nonlinear, which implies that the derivative of J depends on the ocean state. While it is possible to construct the adjoint of the full nonlinear system to provide this derivative information, such an analysis is beyond the present
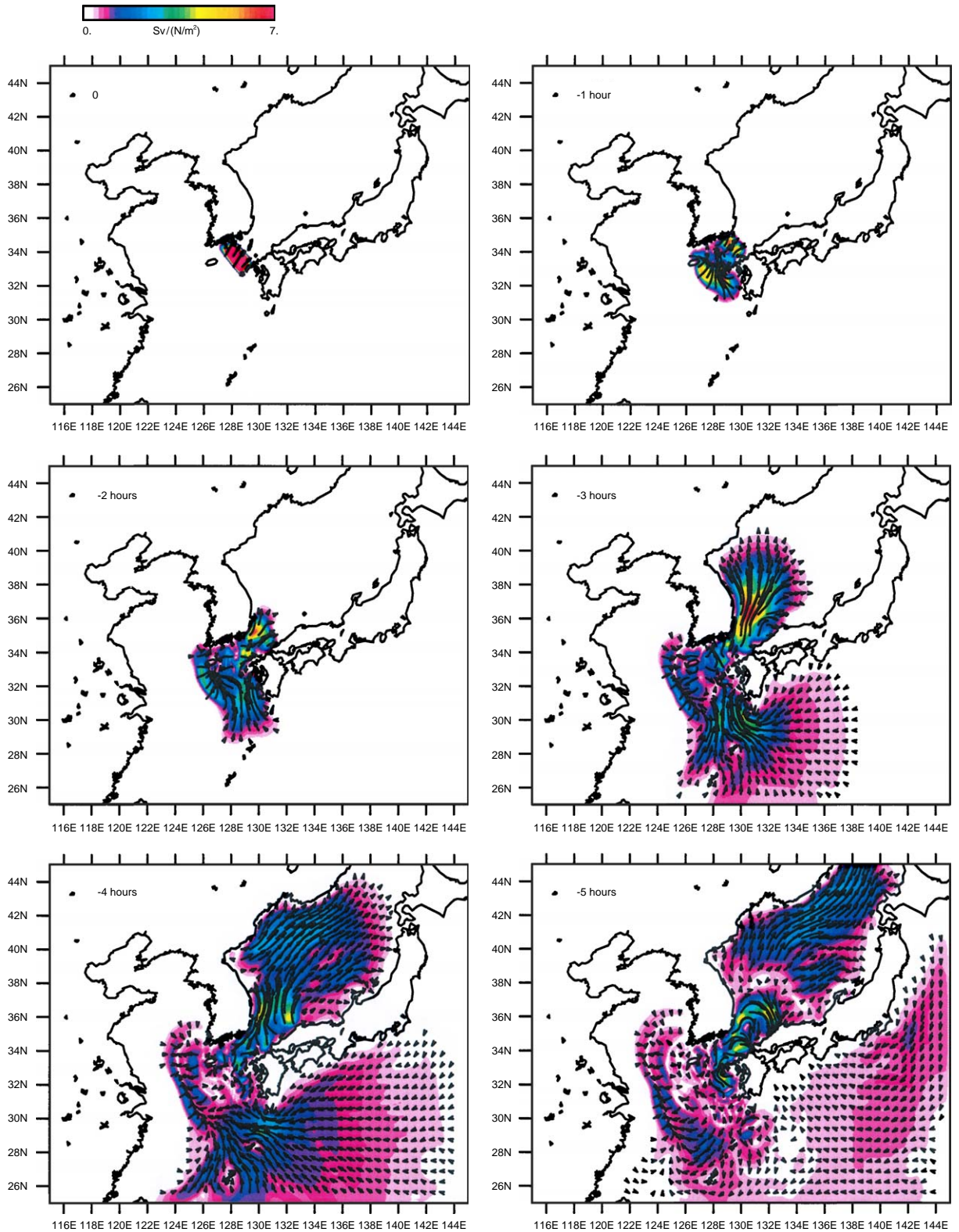
scope of this work. Thus, the simplified linear barotropic adjoint provides the dynamics to examine the strait transport sensitivity to wind stress.

At zero time lag, the adjoint experiment indicates that the derivative of strait transport with respect to wind stress is zero everywhere except at the points where transport is measured (Plate 4). The implication is that at zero time lag the strait transport is sensitive to wind stress only within the strait itself. This situation is expected since the effect of forcing at one point in the ocean requires time to propagate to a distant point. At zero lag the wind-stress effects at points away from the strait have not propagated to the strait.

The units of the vectors in the adjoint derivative plots are equal to the derivative of the transport with respect to wind stress, or Sv per N/m^2. To determine the transport generated by a wind field that occurs at a particular time lag, multiply the derivative vectors at the desired lag by the wind-stress field and integrate over space. There are some small scale features in the derivative results (Plate 4). The small-scale features indicate that the wind stress would require a very unique small-scale structure in order to produce a transport response at time zero. At the longest time lag presented (5 h), the waves caused by the oscillations in the strait propagate out into the open Pacific Ocean. This indicates that if the wind stress in the open Pacific Ocean happened to have a pattern that matched the small-scale patterns in the derivative plots, then it could feed into a transport change. Because the wind stress generally has larger scales, the small-scale structure in the sensitivity would not lead to a transport change. It is within the areas of spatially homogeneous derivatives that wind stress would be most likely to influence the strait transport.

At 2 h lag, the wind stress just northeast of the strait is the most important for determining transport along with the wind stress directly south of the strait. At 3 h lag, the area of greatest sensitivity (the largest derivative) propagates northward into the JES along the Korea coast and the area of smaller sensitivity south of the strait propagates into the area south of Japan along the shelf break and the open Pacific Ocean. At 4 h lag, the area of greatest sensitivity continues to be the western half of the JES with the secondary area extending off the shelf break into the Pacific Ocean south of Japan.

5. Discussion

As discussed in Section 3, the NCOM solution has a positive correlation to the in situ observations. The model is forced by wind stress and does not assimilate data to provide the synoptic mesoscale circulation. Thus, the agreement between model and observations is due to deterministic wind-driven variations. However, the mechanical connection from the wind stress to the strait transport is not immediately apparent.

According to the lagged cross-covariance analyses, the wind stress is most related to the transport through the strait at time lags between -0.5 and -1 day (Figs. 3 and 4). At this lag, the wind stress across the Yellow and East China Seas as well as the JES appears influential. Southerly wind stress and increased northward transport are significantly correlated. The problem of the atmosphere large-scale nature first appears in this analysis. Transport through the Korea Strait is significantly correlated to the wind stress over the Asian land mass. There are few (if any) physical mechanisms that directly link wind stress over the Asian continent to changes in the Korea Strait transport on synoptic scales. Thus, the results of the direct covariance analysis should be viewed as providing only evidence that southerly wind stress over either (or both) the Yellow Sea or the JES at a

Plate 4. The adjoint model is used to determine the derivative of the strait transport with respect to wind stress at varying time lag. The transport induced at time zero by a wind field at a particular time lag is given by the inner product of the wind stress with the derivative shown summed over the domain. For example, only wind stress in the strait at time lag zero affects the transport at time zero. The areas over which the transport is most sensitive to wind stress rapidly propagate northward into the Japan/East Sea and southward along the shelf break. Wind stress over the shelf areas in the Yellow and East China Seas does not greatly influence the strait transport.

time lag of −1 day forces transport variations through the Korea Strait.

The temporal variations in covariance are also of importance. From time lag −2 to 0 days, the area of largest covariance propagates southward from the northern Yellow Sea to the East China Sea. This is related to the typical atmospheric features in this area, which are fronts moving from the northeast to the southwest during winter in particular (Jacobs et al., 1998). Thus, in a manner similar to the large-scale spatial nature of atmospheric forcing, there are large-scale temporal correlations. The area of correlation would be expected to propagate in a manner similar to the features in the atmosphere.

The lagged T/P sea level covariance (Plates 1 and 2) provides some additional insight. The most significant covariance occurs at −1 day lag as in the wind stress, but the area of largest magnitude correlation is in the JES. An increased transport is associated with a sea level set down along the east Korea coast. In addition to the T/P observed sea-level correlations, the NCOM sea-level is correlated to its transport in the same manner (Plate 3). The similarity in the observed T/P and model analyses adds credibility to both. The numerical model indicates that a sea-level drop along the east Korea coast precedes a transport increase. The area of sea-level drop propagates to the south along the Korea coast and moves along the southern Korean coast through the strait. The geostrophic current associated with such a sea-level change would be expected to increase transport through the strait. A second area of positive SSH correlation to transport occurs along the East China Sea shelf break in the numerical model at time lags of −1.0 to 0 days (Fig. 3), and some indications of this correlation are apparent in the observed sea-level correlation (Plates 1 and 2).

The adjoint solution (Plate 4) leads to two important results. First, transport through the strait is not sensitive to wind stress across the Yellow and East China Seas. The wind stress over the shelf areas of the Yellow and East China Seas plays little role in determining the transport through the strait. The derivative of the strait transport with respect to wind stress is computed by the adjoint through the dynamical equations.

Thus, the dynamical equations indicate that wind-stress information does not propagate eastward from the central Yellow and East China Seas to the Korea Strait. Rather, the dynamics propagate wind-stress information more readily from the down-stream area in the JES to the strait. Even as far out as 5 h lag, the influence of wind stress from the shelf areas in the Yellow and East China Seas is minimal. This remains the case when the adjoint model is run to time periods of several days or longer. A second area of sensitivity also appears. The wind stress across the area east of the shelf break south of Japan is dynamically connected to the strait.

The second result from the adjoint is that the speed with which the wind-stress effects propagate is rapid. The wind-stress sensitivity area expands to the edges of the model domain within 9 hours. This seems inconsistent with the observed covariance analyses between transport and wind stress as well as the covariance analyses between transport and sea level. These covariance analyses indicate peaks near −0.5- and −1.0-day lags. However, the actual transport is derived from the derivative of transport integrated with the wind-field, and the wind-field characteristics of slow southwestward movement provide the consistency between the results.

The two SSH response areas (negative correlation in the JES and positive correlation along the East China Sea shelf break) are similar to the areas of transport sensitivity to wind stress indicated by the linear barotropic adjoint model (Plate 4). However, the adjoint model indicates very short time lags between forcing and response (on the order of hours). The connection between these different results is the movement of atmospheric fronts across the area from the northeast to southwest. These fronts require 2 to 3 days to pass from the Bohai Bay to south of the shelf break. Because the barotropic response is rapid relative to the frontal speed, the area that will first influence the strait transport is the JES just east of the Korea peninsula. As the front progresses to the southwest, the shelf break area south of Japan becomes the more influential area to the strait transport.

The results imply a particular mechanism for connecting wind stress to the Korea Strait transport. Wind stress along the east Korean coast

generates a sea level set down for a southerly wind stress. The sea level propagates to the strait as a Kelvin wave. The sea-level slope across the strait changes, and the geostrophic balance provides increased transport. Wind stress south of Japan contributes similarly. Southeasterly wind stress sets up sea level along the Japan coast; this sea-level anomaly propagates to the strait as a Kelvin wave, and transport once again increases. Northerly wind stress has a similar effect by producing a sea level set up along the east Korean coast, and this creates a decreased transport through the strait. The results obtained here are very similar to studies conducted in the Taiwan Strait (Ko et al., 2003a).

Kelvin wave propagation direction preferentially occurs such that when viewed in the direction of propagation, the coast is to the right in the northern hemisphere. Thus, sea-level perturbations created in the Yellow and East China Seas preferentially propagate southward to the Taiwan Strait. Dynamically, the wind stress across the Yellow and East China Seas does not influence the Korea Strait transport.

6. Conclusions

The NCOM model solutions provide evidence that the synoptic transport variations in the Korea Strait are deterministically related to wind stress. Correlation analyses of observed transports provide an indication of the dynamical mechanisms through which wind stress may be connected to the transport through the Korea Strait. Observations from the T/P satellite and the NCOM model are significantly correlated to transport over an area east of the Korean coast. This area of high correlation propagates southward to the strait. The adjoint experiments provide the sensitivity of transport with respect to wind stress. The most sensitive area is east of the Korean peninsula, and a second area appears south of Japan along the shelf break. Taken together, these tools imply the transport is connected to wind stress over the JES and shelf break regions. Wind stress over the Yellow and East China Seas is not dynamically connected to the strait transport. On synoptic scales, wind stress generates Kelvin waves along

the Korean coast that propagate to the strait. The transport is influenced by wind stress within time scales of 4 h according to barotropic dynamics. Due to the slower southwestward propagation of fronts through the area, the maximal correlation of wind stress to transport appears at a −0.5 to −1.0 day lag.

References

Bendat, J.S., Piersol, A.G., 1986. Random Data Analysis and Measurement Procedures. Wiley, New York.

Blumberg, A., Mellor, G., 1987. A description of a three-dimensional coastal ocean circulation model, in three-dimensional coastal ocean models. In: Heaps, N.S. (Ed.), Coastal Estuarine Science, vol. 4. AGU, Washington, D.C., pp. 1–16.

Fox, D.N., Teague, W.J., Barron, C.N., Carnes, M.R., Lee, C.M., 2002. The modular ocean data assimilation system (MODAS). Journal of Atmospheric and Oceanic Technology 19 (2), 240–252.

Fu, L.L., Christensen, E.J., Yamarone, C.A., Lefebvre, M., Menard, Y., Dorrer, M., Escudier, P., 1994. TOPEX/POSEIDON mission overview. Journal of Geophysical Research 99, 24,369–24,382.

Hogan, T.F., Brody, L.R., 1993. Sensitivity studies of the navy global forecast model parameterizations and evaluation of improvements to NOGAPS. Monthly Weather Review 121, 2373–2395.

Hogan, T.F., Rosmond, T.E., 1991. The description of the navy operational global atmospheric prediction system. Monthly Weather Review 119, 1786–1815.

Hsueh, Y., 1988. Recent current observations in the eastern Yellow Sea. Journal of Geophysical Research 93, 6875–6884.

Jacobs, G.A., Teague, W.J., Riedlinger, S.K., Preller, R.H., Blaha, J.P., 1998. Sea surface height variations in the Yellow and East China Seas, 2, SSH variability in the weekly and semiweekly bands. Journal of Geophysical Research 103, 18,479–18,496.

Jacobs, G.A., Perkins, H.T., Teague, W.J., Hogan, P.J., 2001. Summer transport through the Tsushima-Korea Strait. Journal of Geophysical Research 106, 6917–6930.

Ko, D.S., Preller, R.H., Jacobs, G.A., Tang, T.Y., Lin, S.F., 2003. Transport reversals at Taiwan Strait during October and November 1999. Journal of Geophysical Research 108 (C11).

Marchuk, G.I., 1994. Adjoint equations and analysis of complex systems. Kluwer Academic Publishers, Boston.

Martin, P. J., 2000. Description of the navy coastal ocean model version 1.0. Naval Research Laboratory Report NRL/FR/7322—00-9962, 42 pp.

Mellor, G.L., Yamada, T., 1974. A hierarchy of turbulence closure models for planetary boundary layers. Journal of Atmospheric Science 31, 1791–1806.

Mizuno, S., Kawatate, K., Miita, T., 1986. Current and temperature observations in the east Tsushima channel and the Sea of Genkai. Progression Oceanography 17, 277–295.

Ohshima, K.I., 1994. The flow system in the Japan Sea caused by a sea level difference through shallow straits. Journal of Geophysical Research 99 (C5), 9925–9940.

Perkins, H.T., Teague, W.J., Jacobs, G.A., Chang, K.I., Suk, M.S., 2000. Currents in Korea-Tsushima Strait during summer 1999. Geophysical Research Letters 27, 3033–3036.

Rosmond, T.E., 1992. The design and testing of the navy operational global atmospheric prediction system. Weather Forecasting 7, 262–272.